JOURNAL OF GEOPHYSICAL RESEARCH, VOL. 106, NO. A11, PAGES 25,489–25,501, NOVEMBER 1, 2001

Fluid and kinetics signatures of reconnection at the dawn tail magnetopause: Wind observations

Tai D. Phan

Space Sciences Laboratory, University of California, Berkeley, California, USA

Bengt U. Ö. Sonnerup

Thayer School of Engineering, Dartmouth College, Hanover, New Hampshire, USA

Robert P. Lin

Space Sciences Laboratory, University of California, Berkeley, California, USA

Abstract. We report an accelerated plasma flow event detected by Wind at the low-latitude dawn tail magnetopause (x_{GSE}≈-10 R_E) when the local magnetic shear across the magnetopause was high (~180°) and the GSM y component of the interplanetary magnetic field was positive and much larger than the z component. High time resolution (3 s) three-dimensional ion and electron distributions were obtained for this event. We have performed rigorous tests of fluid and particle predictions of reconnection. Consistent with reconnection, we observed at the magnetopause (1) jetting of plasma, with a flow speed, measured in the deHoffmann-Teller frame, at 98% of the Alfvén speed; (2) mixing of a nearly isotropic hot plasma sheet ion distribution with a field-aligned magnetosheath distribution having a low-energy cutoff at the predicted deHoffmann-Teller velocity; (3) opposite streaming of magnetosheath and plasma sheet electrons consistent with open field topology; and (4) a finite inward (earthward) directed normal magnetic field (B_N<0) at and an associated earthward plasma flow (at 94% of the normal Alfvén speed) across the magnetopause. The combined fluid and particle signatures provide a comprehensive set of evidence for reconnection at the magnetopause. These reconnection signatures were observed in the tail flank magnetopause, where the presence of fast plasma flow (at almost twice the local Alfvén speed) in the adjacent magnetosheath has been predicted to suppress reconnection. The sense of the flow enhancement, the direction of the electron heat flux, and the polarity of B_N are all consistent with each other and with the spacecraft being located tailward and northward of the reconnection site. Our analysis places the reconnection site ~7 Earth radii south of the magnetic equator. The dimensionless reconnection rate at this flank magnetopause is estimated to be in the range of 0.1 to 0.2, which is similar to values reported for the subsolar region. In essence, the present event provides unambiguous evidence for reconnection and shows that reconnection signatures at the tail flank magnetopause are not noticeably different from those predicted and observed in the subsolar region.

1. Introduction

Magnetic reconnection is a universal plasma process which converts stored magnetic energy into kinetic and thermal energies. It also creates topological changes which provide access of one plasma to another and is believed to be one of the dominant processes by which solar wind energy is transferred into the Earth's magnetosphere [e.g., *Dungey*, 1961; *Cowley*, 1984].

At the dayside magnetopause, reconnection between magnetosheath and geomagnetic field lines is expected to produce (1) a finite magnetic field component normal to the magnetopause, B_N, [*Sonnerup and Ledley*, 1979]; (2) Alfvénic plasma flow acceleration associated with a rotational discontinuity at the magnetopause [*Levy et al.*, 1964]; (3) ion distributions on reconnected field lines consisting of a mixture of magnetosheath and magnetospheric populations where the transmitted magnetosheath population has a "D-shaped" distribution, with a low-energy cutoff at the deHoffmann-Teller velocity [*Cowley*, 1982]; (4) reflected ions in the layers adjacent to the magnetopause [*Sonnerup et al.*, 1981]; (5) opposite streaming along reconnected field lines of outgoing magnetospheric electrons and incoming magnetosheath electrons, resulting in large parallel electron heat flux; and (6) an offset between the ion and electron edges at the inner boundary of the low-latitude boundary layer (LLBL) due to a time-of-flight effect resulting from the fact that entering magnetosheath electrons have much higher parallel speeds than ions while their transverse motions are the same [*Gosling et al.*, 1990b]. The second expectation represents a macroscopic (fluid) property, while predictions 3 to 6 are kinetic manifestations of reconnection. The sense of B_N, v_N, the directions of both the accelerated flows and the electron heat flux, as well as the form of the D-shaped ion distributions are mutually related and depend on the location of the observation site relative to the reconnection site. The percentage of reflected ions depends on the magnetopause structure and cannot be uniquely predicted theoretically, while the offset between the ion and electron edges is

Paper number 2001JA900054.
0148-0227/01/2001JA900054$09.00

a function of the distance from the observation point to the reconnection site.

Experimentally, B_N is difficult to measure accurately because doing so requires a precise determination of the magnetopause normal. Because the field component tangential to the magnetopause is substantially larger than the normal component, even a slight error in the magnetopause normal determination could lead to large errors in the value of B_N. Thus a measured nonzero B_N in itself is usually not considered to be unambiguous evidence for reconnection.

Reports of plasma jetting that satisfies tangential stress balance across a rotational discontinuity (the so-called Walén test) [e.g., *Paschmann et al.*, 1979, 1986; *Sonnerup et al.*, 1981, 1987; *Gosling et al.*, 1982, 1986, 1991; *Phan et al.*, 2000] have provided quantitative verification of the fluid signatures of reconnection, while observations of kinetic signatures lend further support for the occurrence of reconnection at the dayside magnetopause. These signatures include (1) "D-shaped" ion distributions [e.g., *Gosling et al.*, 1990b; *Smith and Rodgers*, 1991; *Fuselier et al.*, 1991]; (2) opposite streaming magnetosheath and magnetospheric electrons [e.g., *Ogilvie et al.*, 1984; *Mitchell et al.*, 1987]; (3) reflected ions next to the magnetopause [e.g., *Sonnerup et al.*, 1981; *Scholer and Ipavich*, 1983; *Fuselier et al.*, 1991; *Gosling et al.*, 1991]; and the separation of the electron edge from the ion edge at the inner LLBL [Gosling et al., 1990b].

Despite the large amount of evidence for reconnection, open questions remain. Many dayside magnetopause crossings have failed to display flow acceleration with the predicted magnitudes, even under favorable (southward) interplanetary magnetic field (IMF) conditions [e.g., *Papamastorakis et al.*, 1984; *Paschmann et al.*, 1986; *Gosling et al.*, 1990a; *Phan et al.*, 1996]. Furthermore, few reconnection events display all the predicted fluid and kinetic signatures and the presence of a finite B_N. A survey performed by *Bauer et al.* [1998] to check the consistency between the various fluid and particle signatures revealed that although particle signatures are sometimes observed together with the fluid signatures, more often one signature is observed without the other. For example, the majority of accelerated flow events do not display the predicted "D-shaped" ion distributions. The reverse situation also occurs where the observed ion and electron particle signatures are as predicted, but the flow enhancement is substantially below the predicted Alfvén speed. Without clear explanations for these inconsistencies, our understanding of the reconnection process remains incomplete.

In the present study we perform rigorous tests of reconnection predictions on a dawn flank magnetopause crossing by Wind for which high time resolution (3 s) full three-dimensional (3-D) ion and electron distributions are available. The observed fluid and particle characteristics are in quantitative agreement with predictions and together provide compelling evidence for reconnection. This study also reveals possible reasons for the inconsistencies between fluid and particle signatures reported in previous studies. Finally, this reconnection event was detected at the dawn tail flank. The majority of previously detected tail flank reconnection events were on the duskside [*Gosling et al.*, 1986].

2. Instrumentation and Data Selection

The present analysis uses data from the Wind spacecraft. Plasma parameters were obtained from the 3-D Plasma (3DP) detectors [*Lin et al.*, 1995], with varying time resolution. Full 3-D ion distributions were produced every spacecraft spin period (3 s). Because of limited telemetry capacity, the 3-s distributions are usually averaged over 24 or 51 s before being transmitted; however, burst mode data, which provides 6 min of full temporal resolution (3 s) 3-D ion and electron distributions, are available for the magnetopause event reported here. The burst mode is triggered at the magnetopause by sudden changes in the ion flux level. The magnetic field is measured at a rate of 10.9 samples s^{-1}, but for our analysis, the magnetic field data are averaged over 3 s [*Lepping et al.*, 1995].

Plate 1 shows the trajectories of the Wind and the IMP 8 spacecraft during the event. Wind was crossing the dawn tail magnetopause (x_{GSE}= -10 R_E) below the GSM equatorial plane (z_{GSM}= -6.6 R_E) while IMP 8 remained in the dusk tail magnetosheath, providing shocked solar wind plasma and magnetic field information.

The (local) boundary normal (LMN) coordinate system is used throughout this paper. It is defined such that the N axis points outward along the magnetopause normal and the (L, M) plane is tangential to the magnetopause with L oriented approximately due north and M oriented due west (see Figure 1). The magnetopause normal is taken from Fairfield's magnetopause model [*Fairfield*, 1971], except in the determination of B_N (section 4.4), where variance analyses of the measurements are performed.

3. Observations

Plate 2 shows an overview of the Wind outbound pass from the magnetosphere to the magnetosheath on January 13, 1996. In the magnetosphere (i.e., before 2030 UT) the M component of the magnetic field, B_M, is large and positive (Plate 2i), consistent with the spacecraft being located south of the neutral sheet and the magnetospheric field lines being highly stretched. From 2030 to 2100 UT the spacecraft crossed the dawn flank magnetopause multiple times, and high-speed flows were detected (Plate 2c). The peak flow speed is larger than the magnetosheath flow speed by ~200 km s^{-1}. At these times the IMP 8 spacecraft was in the dusk flank magnetosheath and measured a rather constant magnetosheath flow speed (red line in Plate 2c), which implies that the plasma jets detected by Wind at the dawn magnetopause are true flow accelerations unrelated to solar wind velocity variations.

Plate 2l shows the density of the energetic ion and electron populations of magnetospheric origin. It is noted that the sharpest drop of the energetic particle density did not occur at the first encounter of the magnetopause (at ~2030 UT). It occurred much later at ~2110 UT, which coincides with the last magnetopause and high-speed flow encounter.

Plate 2k displays the magnetic field clock angle measured by IMP 8 and Wind. As expected, the clock angle measured by Wind in the dawn magnetosheath (after 2100 UT) agrees well with that in the dusk magnetosheath, indicating that the IMF clock angle has the same value, ~ 90°. The clock angle measured by IMP 8 indicates that the GSM y component of the IMF was much larger than the GSM z component for more than 4 hours surrounding the Wind magnetopause crossing. The magnetosheath and the magnetospheric fields at the dawn tail magnetopause (at the Wind location) are nearly antiparallel.

Plate 3 shows one of the magnetopause crossings in more detail. This event is chosen for detailed analysis because of the availability of the highest resolution (3 s) particle distribution data. The spacecraft was in the magnetosphere at 2030:00 UT. It crossed the entire magnetopause and its boundary layer in less than 2 min and entered the magnetosheath at ~2031:40 UT. Reversing the spacecraft travel direction, the flow enhancements (relative to the mag-

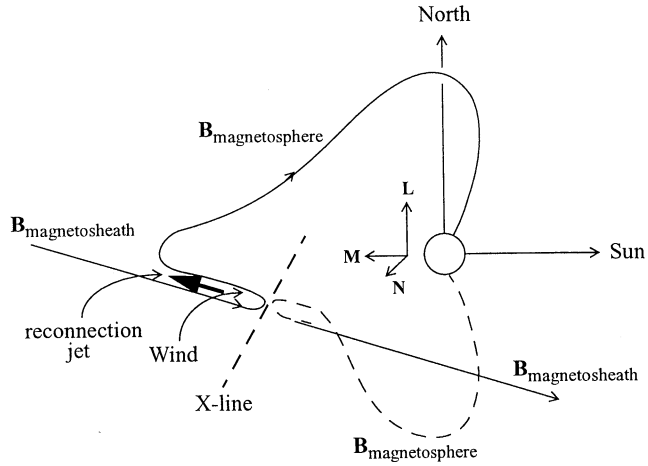

Figure 1. A sketch illustrating reconnection at the dawn tail magnetopause. Our analysis indicates that the Wind satellite crossed the magnetopause in the Southern Hemisphere, tailward and northward of the reconnection site, and the X-line makes an angle of ~60° relative to the equator (with the northern part of the line pointing toward the Sun). The accelerated flows at the magnetopause are indicated by the thick arrow.

netosheath flow) commenced at the outer edge of the current layer, at ~2031:40 UT. The enhanced flows were detected from 2031:40 to 2030:33 UT (Plate 3c), i.e., throughout most of the magnetopause/low-latitude boundary layer (MP/LLBL). The M and L components of the flow velocity are both positively enhanced (Plates 3d-3e), indicating that the spacecraft was located tailward and northward of the reconnection site, as illustrated in Figure 1. Consistency checks of this picture in terms of the sense of B_N and electron heat flux, the presence of D-shaped ion distributions, and the occurrence of Alfvénic flows are the subject of the remainder of this paper. Finally, based on a v_M enhancement of ~200 km s^{-1} and a v_L enhancement of ~100 km s^{-1} across the magnetopause, we infer that the X-line makes an angle of ~60° relative to the equator.

At the magnetopause the magnetic field magnitude, $|\mathbf{B}|$, is reduced to only ~20% of the magnetosheath and magnetospheric values (Plate 3g). Large dips in $|\mathbf{B}|$ occur at several other magnetopause crossings (see Plate 2g) and are part of the magnetopause structure since they do not occur in the magnetosheath proper (after 2100 UT). Such field depressions are common in the magnetopause [e.g., *Sonnerup and Ledley*, 1979] and have been seen in other reconnection events [e.g., *Paschmann et al.*, 1979; *Gosling et al.*, 1986, 1990a, 1991].

4. Analysis

In this section we quantitatively verify both fluid and kinetic predictions of reconnection for the event in Plate 3, and we demonstrate their mutual consistency. We confirm that the observed bulk flow accelerations are in close agreement with the prediction. We then show the presence of "D-shaped" ion distributions, with the predicted low-energy cutoff at the deHoffmann-Teller velocity. The electron distributions are also shown to be consistent with an open magnetopause and in agreement with the configuration of Figure 1. The presence of a finite inward (earthward) directed B_N and a corresponding inward plasma flow across the magnetopause (which is itself moving earthward) is confirmed by two separate methods. On the other hand, some predicted kinetic signatures, namely reflected ions and separate electron and ion edges at the inner LLBL, were not observed in this event. Finally, the magnetopause and LLBL thicknesses, the reconnection rate, as well as the location of the reconnection site are estimated from the knowledge of the speed of the magnetopause boundary itself, the flow across the magnetopause, and the normal magnetic field.

4.1. Tangential Stress Balance

For a rotational discontinuity at the magnetopause [*Levy et al.*, 1964], ideal MHD predicts that the reconnection flow is Alfvénic in the deHoffmann-Teller (HT) frame of reference [*Sonnerup et al.*, 1987]. This condition is called the Walén relation and is expressed as

$$\mathbf{v} - \mathbf{V}_{HT} = \pm(1-\alpha)^{1/2}\,\mathbf{B}/(\mu_0\rho)^{1/2}, \quad (1)$$

where $\mathbf{v}$ is the plasma velocity, $\mathbf{V}_{HT}$ is the deHoffmann-Teller velocity, $\mathbf{B}$ is the magnetic field, and ρ is the total mass density. Also, the pressure anisotropy factor is $\alpha = (p_{\parallel} - p_{\perp})\mu_0/B^2$, where $p_{\parallel}$ and $p_{\perp}$ are the plasma pressures parallel and perpendicular to $\mathbf{B}$, respectively.

4.1.1. Existence of the deHoffmann-Teller frame. The existence of a finite B_N at the magnetopause requires field lines on both sides of the magnetopause to move together. In this scenario there must be a reference frame (the HT frame) which slides along the magnetopause with the field line velocity. In this frame the convective electric field vanishes ($\mathbf{E}_c = -\mathbf{v}\times\mathbf{B} = 0$); that is, the flows are field-aligned on the two sides of the magnetopause.

The HT frame for a set of plasma and field measurements can be found as the reference frame in which the mean square of the convective electric field, $D = \langle|(\mathbf{v} - \mathbf{V}_{HT})\times\mathbf{B}|^2\rangle$, is as small as possible [*Sonnerup et al.*, 1987; *Khrabrov and Sonnerup*, 1998c]. The angle bracket $\langle\ \rangle$ denotes an average of an enclosed quantity over a set of measurements. The velocity $\mathbf{v}$ for which $D(\mathbf{v})$ is a minimum is the deHoffmann-Teller velocity, $\mathbf{V}_{HT}$. The ratio D/D_0, where $D_0 = \langle|(\mathbf{v}\times\mathbf{B}|^2\rangle$, is often used as a measure of the quality of the HT frame. For a good HT frame, D/D_0 should be small ($\ll 1$). The quality of the HT frame for a data interval is also evident when a single velocity $\mathbf{V}_{HT}$ can be found such that $-\mathbf{v}^m\times\mathbf{B}^m \sim -\mathbf{V}_{HT}\times\mathbf{B}^m$, where the superscript m denotes individual data points in the interval.

We compute the deHoffmann-Teller velocity using the method by *Sonnerup et al.* [1987] for the 2031:10-2031:42 UT interval indicated by the green bars in Plate 3. This interval includes a segment of the enhanced flow region and a few magnetosheath measurements in the immediate vicinity of the magnetopause. Analyses in section 4.4 suggest that this is the optimal data interval for the determination of the magnetopause normal vector. One obtains $\mathbf{V}_{HT} = (-185\mathbf{x}, -89\mathbf{y}, 71\mathbf{z})_{GSE}$ km s^{-1}. When $-\mathbf{v}^m\times\mathbf{B}^m$ is plotted against $-\mathbf{V}_{HT}\times\mathbf{B}^m$ (Plate 4a), the best fit of the data points has a slope of +1.06 and a correlation coefficient of 0.96. Together with the ratio $D/D_0 = 0.06$ these results indicate the existence of a good HT frame.

4.1.2. Walén test. Plate 4b shows the scatterplot of each GSE x, y, and z component of the flow velocity in the HT frame versus the Alfvén velocity. On average, the flow speed in the HT frame is 98% of the Alfvén speed, and the correlation coefficient R between the two quantities is 0.93. The pressure anisotropy factor α is small in this event and is not an important factor in the Walén test. The positive slope of the regression line implies that the normal magnetic field points earthward (i.e., $B_N<0$) [e.g., *Sonnerup et al.*, 1981], consistent with the scenario in Figure 1.

The results of the tangential stress balance test are not sensitive to the chosen data interval as long as the interval does not include

samples in the innermost region of the LLBL. Plate 5 shows the Walén slope and the correlation coefficient as one varies the data interval. In this analysis the outer (magnetosheath) edge of the interval is fixed (at 2031:42 UT) while the inner (LLBL) edge is varied between 2030:00 and 2031:38 UT. Results in Plate 5 are shown as a function of the time which corresponds to the LLBL edge of the data interval. The Walén slope (Plate 5b) and the correlation coefficient R (Plate 5c) are excellent (better than 0.9) across an extended time interval when the inner edge is in the range of 2030:36-2031:30 UT. It is only when the interval extends earthward of 2030:36 UT that the regression slope and the correlation coefficient decrease substantially below unity. This finding indicates that the region immediately earthward of 2030:36 UT, in which the flow speed remains high, is not governed by the Walén relation: It may represent slow-mode expansion, modified by non-MHD effects. Another complication is present in this region: The density and temperature profiles in Plate 3 suggest that a brief reversal of the magnetopause normal motion occurred in the interval 2030:28-2030:42 UT. Such a boundary motion reversal should not be included in deHoffmann-Teller and Walén analyses. In other words, the earthward edge of the data interval should not be before 2030:42 UT. The poor Walén slope for cases where the inner edge of the interval is after 2031:30 UT, on the other hand, is due to the small number of measurements in these cases (Plate 5d).

Finally, although the ion measurements by the Wind 3DP experiments assume all detected ions to be protons, the ion velocity moment agrees remarkably well with the Walén relation. This indicates that, at least for this event, the effects of heavy ions on the computed moments are negligible.

4.2. Ion Distributions

The kinetic description of reconnection can also be quantitatively verified. An important kinetic signature is the so-called "D-shaped" ion distribution. Magnetosheath particles can either be reflected at or cross the magnetopause. In the deHoffmann-Teller frame of reference in which the electric field vanishes, only ions traveling toward the magnetopause will cross the magnetopause. Thus, when viewed in the spacecraft frame, only magnetosheath ions with parallel velocity greater than the deHoffmann-Teller velocity can be seen earthward of the magnetopause, resulting in a "D-shaped" distribution [*Cowley*, 1982]. Along the reconnected field lines, hot magnetospheric ions are also expected to be present.

Plate 6 shows ion distributions taken in the magnetosphere at 2030:00 UT, in the inner part of the LLBL at 2030:33 UT, in the magnetopause at 2031:17 UT, and in the magnetosheath proper at 2032:34 UT. The distributions in the magnetopause (Plate 6c) contain a mixture of hot magnetospheric and cold magnetosheath populations. While the hot magnetospheric component is nearly isotropic, the magnetosheath component displays a significant shift from the origin toward the +**B** direction and has the characteristic D shape with the low-energy cutoff occurring at the deHoffmann-Teller velocity, in quantitative agreement with prediction. D-shaped distributions, similar to Plate 6c, are visible in 15 consecutive measurements, from 2030:45 to 2031:30 UT, corresponding to most of the flow enhancement region and to the interval when the Walén slope is close to 1. The streaming of particles of magnetosheath origin along the magnetic field (+**B**) direction (Plates 6b and 6c) is consistent with the scenario of Figure 1. As one approaches the innermost portion of the LLBL, however, the cold population appears less "D-shaped" (Plate 6b).

Another kinetic prediction of reconnection is the possible presence of reflected ions in the layers adjacent to the magnetopause [e.g., *Cowley et al.*, 1982]. However, the percentage of reflected particles depends on the magnetopause structure and therefore canot be uniquely predicted theoretically. For the present event the ion distributions sampled in the MP/LLBL and in the magnetosheath in the immediate vicinity of the magnetopause display no evidence for reflected magnetospheric or magnetosheath ions. Thus the percentage of reflected ions must be low in this event, but in other reconnection events the percentage has been found to be higher [e.g., *Sonnerup et al.*, 1981; *Scholer and Ipavich*, 1983; *Fuselier et al.*, 1991; *Gosling et al.*, 1991].

4.3. Electron Distributions

Plate 7 shows electron distributions in the magnetosphere, the magnetopause/LLBL, and the magnetosheath. In the magnetosphere (Plate 7a) the electron phase space densities parallel (0^o) and antiparallel (180^o) to **B** are equal at all energies, indicating that the region is on closed magnetic field lines. The magnetosheath distribution (Plate 7d) is colder and denser than the magnetospheric distribution (Plate 7a). The parallel (black curve), antiparallel (blue curve), and perpendicular (green curve) distributions in the magnetosheath have similar temperatures although the overall antiparallel flux is larger than the parallel and perpendicular fluxes. The enhanced field-aligned fluxes in the magnetosheath indicate the presence of solar wind "strahl" electrons. In the LLBL and MP (Plates 7b and 7c) the parallel and antiparallel distributions have different temperatures. Comparisons with the magnetosheath and magnetospheric distributions indicate that the LLBL/MP distributions represent opposite streamings of hot magnetospheric electrons (antiparallel to **B**) and slightly heated magnetosheath electrons (parallel to **B**). This feature of the electron distribution is detected throughout the enhanced flow region (2030:33-2031:32 UT), indicating that nearly the entire MP/LLBL region is on open field lines. In other words, the field lines appear open even in regions where D-shaped ion distributions are no longer detected and where the Walén test (of the rotational discontinuity) fails. The senses of the magnetosheath and magnetospheric electron streamings are consistent with an inward directed normal magnetic field, $B_N < 0$, at the magnetopause (Figure 1).

A previously reported kinetic signature of reconnection is the presence of an offset between the ion and electron edges at the inner boundary of the LLBL [*Gosling et al.*, 1990b]. This offset is a time-of-flight effect resulting from the fact that entering magnetosheath electrons have much higher parallel speeds than ions while their transverse motions are the same. However, for the present event we found no evidence for an electron edge earthward of the ion edge. Earthward of the LLBL, all detected electron distributions are magnetospheric distributions similar to Plate 7a. This absence of a separation between the electron and ion edges may indicate that the reconnection site is not far from the observation point, a conclusion that is supported by our analysis in section 4.7.

Finally, it should be noted that the electron signatures detected at this high-magnetic shear MP/LLBL are in sharp contrast to the low-shear MP/LLBL, where the electrons typically display well-balanced field-aligned and anti-field-aligned fluxes at all energies (similar to Plate 7a) throughout the LLBL [e.g., *Phan et al.*, 1997], a feature that has been interpreted as evidence for closed field lines in the boundary layer [see also *Mitchell et al.*, 1987; *Traver et al.*, 1991; *Fujimoto et al.*, 1996].

Table 1. Summary of Normal Vectors, Normal Magnetic Field B_N, Boundary Speed $\mathbf{V_{HT}}\bullet\mathbf{n}$, Normal Reconnection Flow $v_{N,rec}$, and Reconnection Rate

Method	n_xGSE	n_yGSE	n_zGSE	B_N, nT	$\mathbf{V_{HT}}\bullet\mathbf{n}$, km s^{-1}	$V_{N,rec}$, km s^{-1}	$\mathbf{v}_A\bullet\mathbf{n}$, km s^{-1}	$\lvert B_N\rvert/\lvert\mathbf{B}\rvert$	$\lvert v_{N,rec}\rvert/v_A$	E_t, mV m^{-1}
MVAB	0.197	-0.689	-0.697	-4.9±1.0	-25.3±9.6	-33.1	-34.8	0.20	0.19	0.80
MFR[b]	0.203	-0.797	-0.569	-2.5±1.5	-7.8±16.0	-16.4	-17.7	0.10	0.08	0.40
MVAE[c]	0.201	-0.798	-0.569	-2.5±0.8	-7.3±8.7	-16.0	-17.4	0.10	0.08	0.40
MVAE[d]	0.193	-0.865	-0.463	-0.5±1.1	7.8±9.1	-2.1	-3.5	0.02	0.01	0.05

[a] MVAB, minimum variance of **B**; MFR, minimization of Faraday residue; MVAE, maximum variance of **E**.
[b] MFR analysis produces a boundary speed $u_{N,MFR}$= -17.7±2.4 km s^{-1}.
[c] MVAE, assuming u_N= $u_{N,MFR}$= -17.7 km s^{-1}.
[d] MVAE, assuming u_N= 0 km s^{-1}.

4.4. Determination of Normal Magnetic Field B_N and Plasma Flow $v_{N,rec}$ Across the MP

All fluid and particle signatures presented so far imply the presence of a finite and negative B_N and $v_{N,rec}$ across the local magnetopause. To confirm the existence of such a flow and field we perform variance analyses to determine the magnetopause normal (which needs to be more accurate than Fairfield's [1971] average magnetopause normal), and subsequently B_N and $v_{N,rec}$. We employ two independent methods and evaluate their findings: (1) minimum variance analysis of the magnetic field [*Sonnerup and Cahill*, 1967; *Sonnerup and Scheible*, 1998] and (2) minimization of the Faraday residue [*Terasawa et al.*, 1996; *Khrabrov and Sonnerup*, 1998b]. The results of the magnetopause normal determination are subject to the following consistency tests: (1) Is the magnetopause motion along its normal inward; that is, is $\mathbf{V_{HT}}\bullet\mathbf{n}$ < 0 (see, for example, Figure 9.2 of *Khrabrov and Sonnerup* [1998c]) consistent with the outbound crossing by Wind? (2) Is the normal flow velocity across the magnetopause $v_{N,rec}$= <**v**•**n**> - $\mathbf{V_{HT}}\bullet\mathbf{n}$ consistent with the expected inward plasma flow across the magnetopause at the predicted Alfvén speed $\mathbf{v}_A\bullet\mathbf{n}$= $(1-\alpha)^{1/2}B_N$ / $(\mu_0\rho)^{1/2}$?

As in the Walén analysis (section 4.1), we first perform the variance analyses on the optimal data segment, 2031:10-2031:45 UT, and then discuss the consequences of varying the data interval.

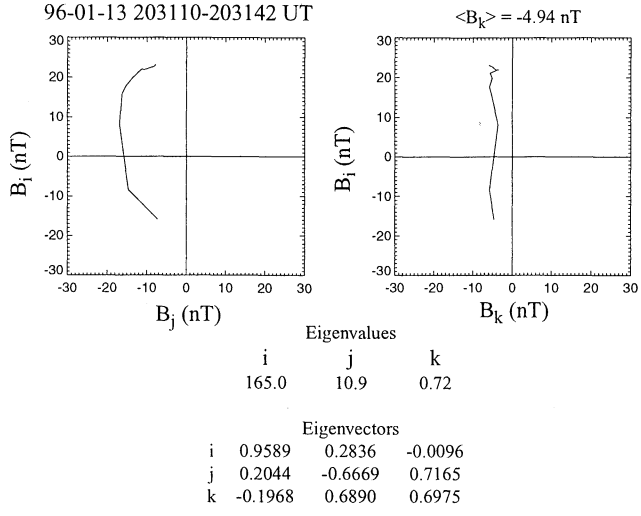

Figure 2. Magnetic structure during MP crossing at 2031:10-2031:42 UT, shown in hodogram form. B_i, B_j, and B_k are field components along the maximum, intermediate, and minimum variance eigenvectors *i*, *j*, and *k*, respectively. Also given are the eigenvalues and eigenvectors.

The summary of the variance analyses on the fixed 2031:10-2031:42 UT data interval is given in Table 1. In the analysis where the data interval is varied, we fix the outer (magnetosheath) edge of the interval (at 2031:42 UT) and vary its inner (LLBL) edge. As discussed in section 4.1, to avoid the boundary motion reversal which occurs before 2030:42 UT and to ensure that a sufficient number of measurements (say, more than four measurements) are contained in the analysis, we vary the inner edge of the interval between 2030:42 and 2031:30 UT.

4.4.1. Minimum variance of B (MVAB). The minimum variance analysis on the fixed 2031:10-2031:42 UT data interval gives the normal vector $\mathbf{n}_{MVAB}$= (0.197**x**, -0.689**y**, -0.697**z**)$_{GSE}$ and the corresponding $B_{N,MVAB}$= -4.9 ± 1.1 nT. The uncertainty in $B_{N,MVAB}$ was estimated using a method by *Khrabrov and Sonnerup* [1998a]. The eigenvalues corresponding to the maximum, intermediate, and minimum variances are e_i= 165, e_j= 10.9, and e_k= 0.72, respectively. The ratio of intermediate to minimum eigenvalue is e_j/e_k=15, indicating that the minimum variance direction, and hence the normal vector, is rather well determined. The magnetic hodograms are shown in Figure 2. The negative value of $B_{N,MVAB}$ is consistent with the scenario of Figure 1. The finding of a negative B_N is robust because it is not sensitive to the data interval chosen. As we vary the inner edge of the data interval, Plate 8b shows that $B_{N,MVAB}$ remains negative. The magnitude of $B_{N,MVAB}$, however, varies by about a factor of 2 (-8 to -4 nT) as the data interval is varied.

In order to check the quality of the MP normal determination, we first examine whether the computed magnetopause motion along its normal, $\mathbf{V_{HT}}\bullet\mathbf{n}$, is consistent with the sense of spacecraft crossing of the magnetopause. Using data in the 2031:10-2031:42 UT interval, one obtains $\mathbf{V_{HT}}\bullet\mathbf{n}_{MVAB}$= -25.3 ± 9.6 km s^{-1}. The negative value of the normal velocity indicates inward motion of the MP, consistent with the outbound MP crossing by Wind. As we vary the inner edge of the data interval, Plate 8c shows that $\mathbf{V_{HT}}\bullet\mathbf{n}_{MVAB}$ remains negative. Similar to $B_{N,MVAB}$, the boundary velocity varies by about a factor of 2 (-40 to -20 km s^{-1}) depending on the data interval chosen.

The next, more quantitative consistency test consists of examining whether the reconnection flow across the magnetopause, $v_{N,rec}$, and the normal magnetic field B_N are related through the rotational discontinuity condition, namely $v_{N,rec}$= $\pm(1-\alpha)^{1/2}B_N/(\mu_0\rho)^{1/2}$. We obtain $v_{N,rec}$ by subtracting the measured normal flow velocity component **v**•**n** averaged over the reconnection layer (which we take to be the interval marked by green bars in Plate 3) from the normal boundary velocity component $\mathbf{V_{HT}}\bullet\mathbf{n}$. For the 2031:10-2031:42 UT interval, <**v**•$\mathbf{n}_{MVAB}$>= -58.4 km s^{-1}, $\mathbf{V_{HT}}\bullet\mathbf{n}_{MVAB}$= -25.3 km s^{-1}, thus $v_{N,rec,MVAB}$= -33.1 km s^{-1}. The negative sign of $v_{N,rec}$ is consistent with inward magnetosheath flows from the magnetosheath, and the agreement of its sign with that of B_N is

consistent with the scenario of Figure 1. The normal Alfvén speed is computed with a magnetosheath density of 8.5 cm^{-3} (see the blue bar interval in Plate 3) and $B_{N,MVAB}$ value of -4.9 nT, giving $\mathbf{v}_A \cdot \mathbf{n}$= -34.8 km s^{-1}. Thus $v_{N,rec,MVAB}$ is 94% of the normal Alfvén speed. As we vary the inner edge of the data interval from 2030:42 to 2031:30 UT, Plate 9b shows that the agreement between $v_{N,rec,MVAB}$ and $\mathbf{v}_A \cdot \mathbf{n}$ remains good (better than 80%) for this entire range of data interval.

4.4.2. Minimization of Faraday residue (MFR). *Terasawa et al.* [1996] proposed a technique in which the constancy of the normal component of the magnetic field and that of the tangential electric field are both satisfied in a single optimization that yields the normal vector as well as the MP boundary speed. Employing the analytical method of *Khrabrov and Sonnerup* [1998b] for the fixed 2031:10-2031:42 UT interval, one obtains a normal vector $\mathbf{n}_{MFR}$= (0.203**x**, -0.797**y**, -0.569**z**)$_{GSE}$, which forms an angle of 9.7° with $\mathbf{n}_{MVAB}$. The normal magnetic field is $B_{N,MFR}$= -2.5 ± 1.5 nT, where the error in $B_{N,MFR}$ has been estimated in a manner similar to the method of *Khrabrov and Sonnerup* [1998a]. The eigenvalues in this case are e_i= 1.86×10^{-6}, e_j= 9.48×10^{-7}, and e_k=6.22×10^{-8}. The ratio of intermediate to minimum eigenvalue is e_j/e_k=15. Similar to MVAB, the finding of a negative $B_{N,MFR}$ is robust: It does not depend on the choice of data interval (Plate 8d). The magnitude of $B_{N,MFR}$ varies by a factor of ~3 when the inner edge of the data interval is varied between 2030:42 and 2031:30 UT.

The Faraday residue minimization process also yields a MP boundary speed [*Khrabrov and Sonnerup*, 1998b], $u_{N,MFR}$, of -17.7 ± 2.4 km s^{-1}. This value is different from the boundary speed obtained from $\mathbf{V}_{HT} \cdot \mathbf{n}_{MFR}$ = -7.8 ± 16.0 km s^{-1}. The reason for the disagreement is not understood, but the discrepancy is within uncertainties. The negative values of both $u_{N,MFR}$ and $\mathbf{V}_{HT} \cdot \mathbf{n}_{MFR}$ are consistent with the sense of magnetopause crossing. Plate 8e shows that both $\mathbf{V}_{HT} \cdot \mathbf{n}_{MFR}$ and $u_{N,MFR}$ remain negative for most of the data intervals, varying between 0 and -20 km s^{-1}.

We now check the quantitative agreement between the plasma flow velocity across the magnetopause and the normal Alfvén velocity. For the 2031:10-2031:42 UT interval the measured plasma flow velocity normal to the magnetopause is $\langle \mathbf{v} \cdot \mathbf{n}_{MFR} \rangle$= -24.2 km s^{-1}. If we first take the boundary velocity to be $\mathbf{V}_{HT} \cdot \mathbf{n}_{MFR}$= -7.8 km s^{-1}, then the normal flow across the MP due to reconnection is $v_{N,rec,MFR}$= -16.4 km s^{-1}. On the other hand, we find $\mathbf{v}_A \cdot \mathbf{n}_{MFR}$= -17.7 km s^{-1}. Thus $v_{N,rec,MFR}$ is 92% of the normal Alfvén speed. Plate 9d shows the result of $v_{N,rec,MFR}$ and $\mathbf{v}_A \cdot \mathbf{n}_{MFR}$ comparison as the data interval is varied. Similar to MVAB, the agreement between these two quantities is excellent for all data intervals. If the boundary velocity is taken to be $u_{N,MFR}$= -17.7 km s^{-1} instead, we find $v_{N,rec,MFR}$= -6.5 km s^{-1}, a result that is only 37% of $\mathbf{v}_A \cdot \mathbf{n}_{MFR}$. We thus conclude that $\mathbf{V}_{HT} \cdot \mathbf{n}_{MFR}$ is closer to the true MP velocity than $u_{N,MFR}$.

We have also performed maximum variance analysis (MVAE) on the convective electric field to determine the MP normal using the method by *Sonnerup et al.* [1987]. The result of the analysis depends on the assumed magnetopause normal speed. If we assume that u_N= $u_{N,MFR}$= -17.7 km s^{-1} obtained from the MFR analysis, the results of MVAE are nearly identical to those of MFR (see Table 1): a finding which is consistent with the conclusion of *Khrabrov and Sonnerup* [1998b] and which indicates that the MVAE and MFR methods are closely related. If the MP boundary is assumed to be stationary instead, the MVAE analysis produces a large discrepancy between $v_{N,rec}$ and $\mathbf{v}_A \cdot \mathbf{n}$, and the resulting boundary motion ($\mathbf{V}_{HT} \cdot \mathbf{n}$) is outward, inconsistent with the sense of the MP crossing (see Table 1).

4.4.3. Summary of variance analyses. We have obtained magnetopause normal vectors and B_N from two separate methods. Both methods produce negative B_N values, consistent with the scenario of Figure 1. The finding of a negative B_N by both methods is robust in the sense that it is not sensitive to the data interval chosen. The magnitude of B_N, however, differs by a factor of 2 or 3 not only from one method to another but also as the data interval is varied. The large uncertainty in B_N is due to the dominance of the field component tangential to the magnetopause such that a small difference in the magnetopause normal direction leads to a large discrepancy in B_N. Further tests of the accuracy of the normal vector have been performed in hope of revealing which method and what time interval produce the most accurate MP normal vector. We first tested the consistency between the boundary motion given by $\mathbf{V}_{HT} \cdot \mathbf{n}$ and the sense of spacecraft crossing of the magnetopause. Both MVAB and MFR methods produce a negative $\mathbf{V}_{HT} \cdot \mathbf{n}$ consistent with the outbound MP crossing.

We next examined the agreement between the normal flow velocity (in the frame of the moving magnetopause) and the normal Alfvén velocity. The agreement is found to be excellent for both methods and for all data segments even though the normal flow velocity and magnetic field themselves vary from one method to the next and when the data interval is varied. This good agreement indicates that the Walén relation is well satisfied for all three components of the flow and field in any coordinate systems. However, it does not allow the identification of the optimal method or the optimal data interval.

To get an indication of the optimal data interval, we examine the uncertainties in B_N as we vary the data interval. For both the MVAB and MFR methods the uncertainty in B_N is a minimum when the earthward edge of the data interval is set at 2031:10 UT, suggesting that the 2031:10-2031:42 UT data interval gives the most accurate magnetopause normal. On the basis of this interval, we obtained $B_{N,MVAB}$= -4.9 ± 1.1 nT and $B_{N,MFR}$= -2.5 ± 1.5 nT. Thus the difference in the B_N values from the two methods is within uncertainties: The true $B_{N,MVAB}$ is likely to be between -2.5 and -4.9 nT.

4.5. Reconnection Rate

We now estimate the reconnection rate based on the normal magnetic field and plasma flow across the MP obtained from the MVAB and MFR methods. The dimensionless reconnection rate is given by

$$M_{A,N} = |v_{N,rec}|/v_A = |B_N|/|\mathbf{B}|, \quad (2)$$

where the Alfvén speed v_A and the field strength $|\mathbf{B}|$ are measured in the (inflow) magnetosheath region. With a magnetosheath density of ~8.5 cm^{-3} (Plate 3a) and a magnetic field strength of ~25 nT (Plate 3g), the dimensionless reconnection rate $M_{A,N}$ for the 2031:10-2031:42 UT data interval based on MVAB is 0.19 from $|v_{N,rec}|/v_A$ and 0.20 from $|B_N|/|\mathbf{B}|$. Using the MP normal from MFR, one gets instead $|v_{N,rec}|/v_A$= 0.08 and $|B_N|/|\mathbf{B}|$= 0.10. Plate 9 shows the results of this analysis as we vary the earthward edge of the data interval. For MVAB the reconnection rate is in the 0.15-0.3 range, whereas MFR gives a rate of 0.06-0.3.

The reconnection rate expressed in terms of the tangential electric field (E_t= $v_{N,rec}B_t$) is ~0.8 mV m^{-1} for MVAB and ~0.4 mV m^{-1} for MFR when the 2031:10-2031:42 UT interval is used. These values are not significantly different from the average reconnection rate of 0.4 mV m^{-1} reported for the subsolar magnetopause from a large statistical study [*Lindqvist and Mozer*, 1990].

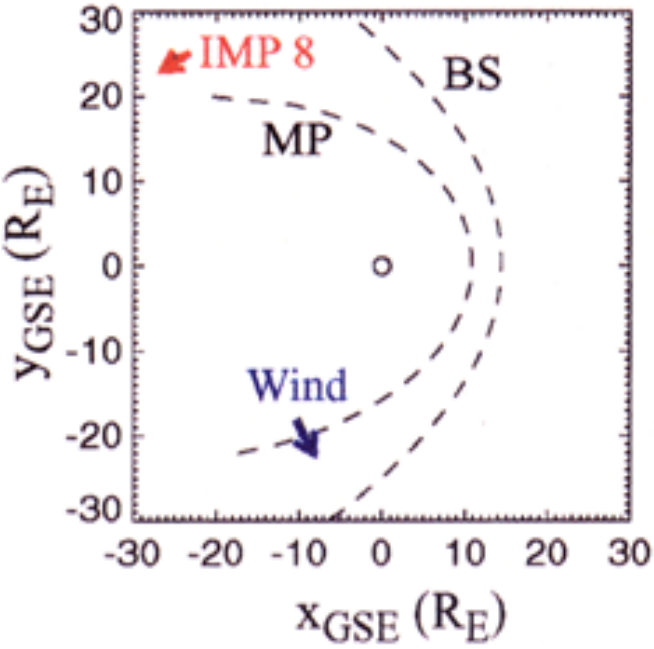

Plate 1. Trajectories of the Wind and IMP 8 spacecraft on January 13, 1996, from 1830 to 2230 UT. Wind crossed the dawn tail flank while IMP 8 remained in the dusk magnetosheath. MP, magnetopause; BS, bow shock.

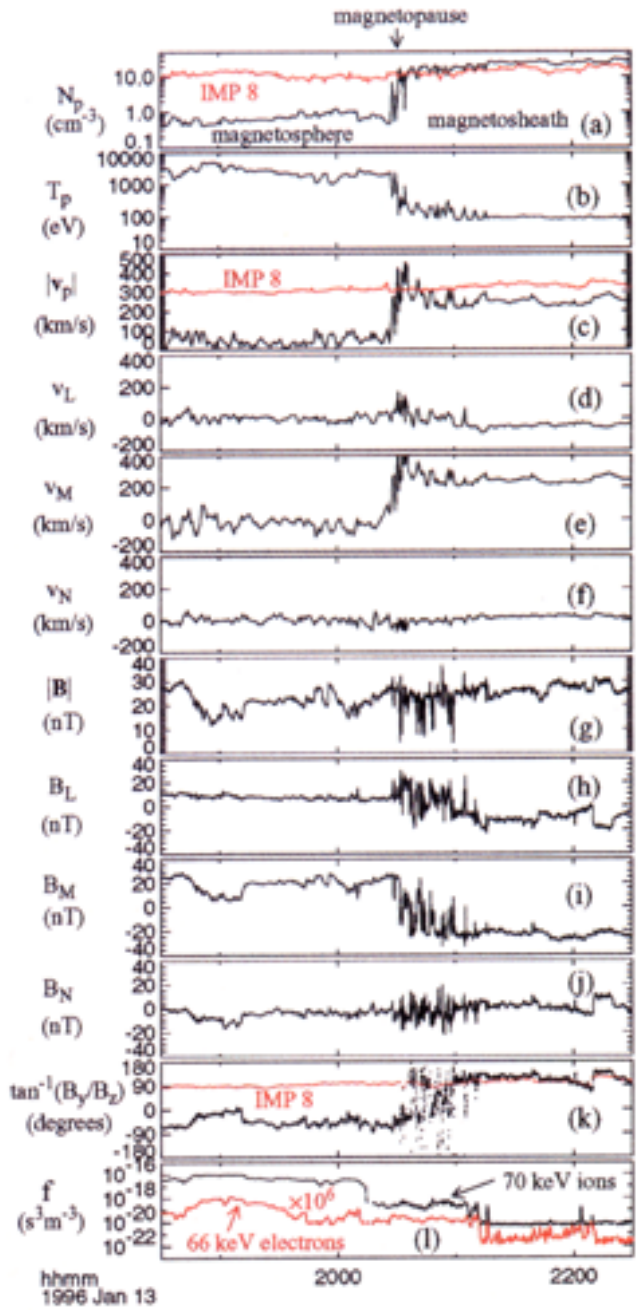

Plate 2. Overview of Wind crossings of the dawn tail magnetopause on January 13, 1996. (a) The ion number density N_p; (b) the ion temperature T_p; (c) the ion bulk speed $|\mathbf{v}_p|$; (d-f) the three components of the ion bulk velocity in the LMN boundary normal coordinate system (see section 2 for definition); (g) the magnetic field strength $|\mathbf{B}|$; (h-j) the L, M, and N components of the magnetic field; (k) the clock angle of the magnetic field; and (l) the energetic ion and electron distribution functions. IMP 8 provided shocked solar wind information at the dusk tail flank (red curves in Plates 2a, 2c, and 2k). The IMP 8 data have been shifted by -260 s.

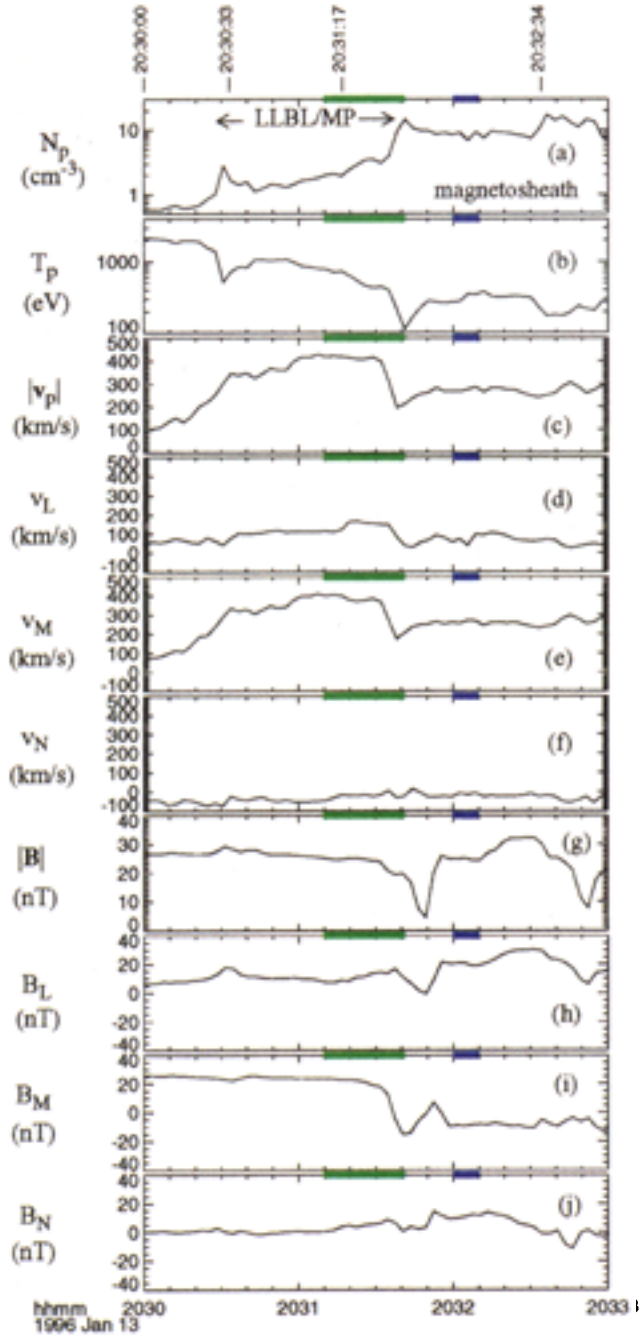

Plate 3. (a-j) Zoom-in of Plate 2 to show one magnetopause crossing (corresponding to the short blue bar interval in Plate 2) in more detail. High time (3 s) resolution particle distributions are available for the entire interval. The subinterval indicated by the green bars, corresponding to the outer MP/low-latitude boundary layer (LLBL), is used in the Walén and minimum and maximum variance analyses. The blue bars indicate the magnetosheath reference interval.

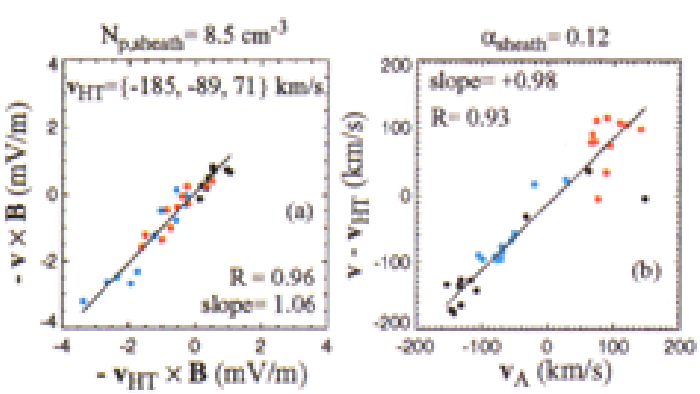

Plate 4. The deHoffmann-Teller and Walén analyses of the outer MP/LLBL for the interval 2031:10-2031:42 UT, marked by a green bar in Plate 3. (a) Scatterplot of the GSE components of $-\mathbf{v}^m \times \mathbf{B}^m$ versus the corresponding components of $-\mathbf{V}_{HT} \times \mathbf{B}^m$. (b) Scatterplot of the GSE components of the flow velocity in the deHoffmann-Teller (HT) frame versus the Alfvén velocity. The black, blue, and red dots denote the *x*, *y*, and *z* components, respectively.

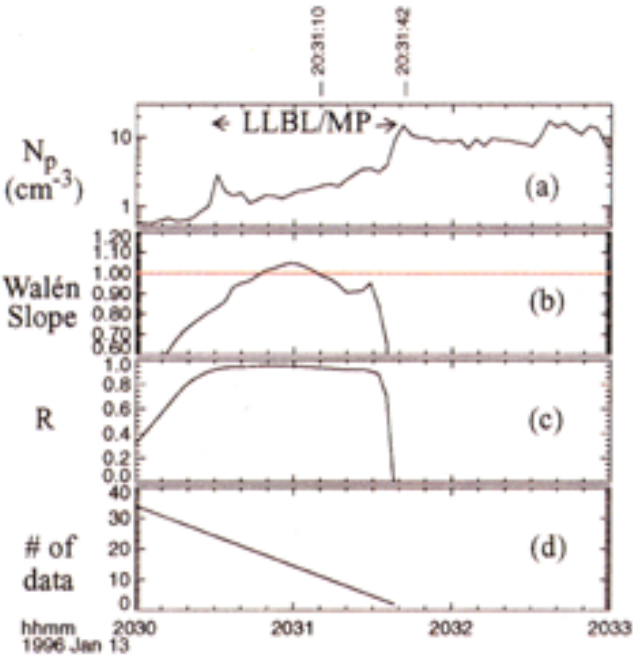

Plate 5. (a-d) Results of the Walén analysis as a function of the "location" of the inner edge of the data interval. The outer edge is fixed at 2031:42 UT. The Walén slope (Plate 5b) is within 10% of the prediction when the inner edge of the interval is between 2030:36 and 2031:30 UT. The Walén slope and the correlation coefficient *R* deviate substantially from unity as more inner LLBL samples (earthward of 2030:36 UT) are included. The bad Walén slope beyond 2031:30 UT is due to the small number of measurements in the interval (Plate 5d).

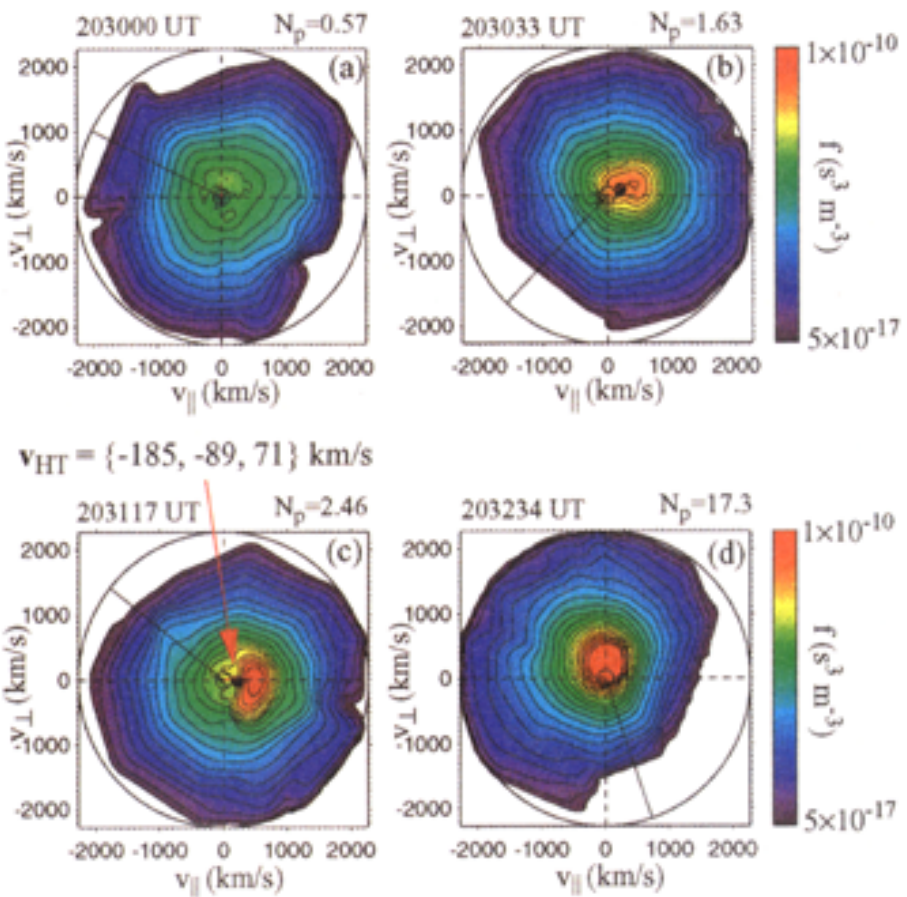

Plate 6. (a-d) Two-dimensional cuts of the ion distributions through velocity space that contains the directions of the magnetic field, **B** (to the right) and **E×B** (upward), sampled in (a) the magnetosphere, (b) the inner LLBL, (c) the outer LLBL/MP, and (d) the magnetosheath proper. The projection of the sunward direction is marked by the black line. The black dot in Plates 6b and 6c denotes the deHoffmann-Teller velocity.

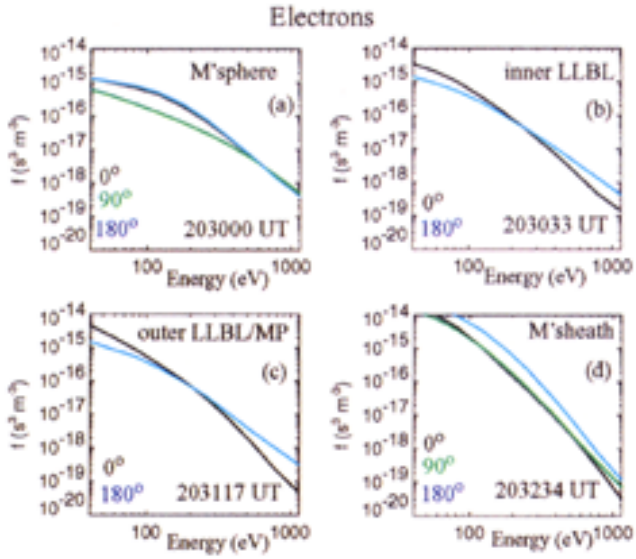

Plate 7. One-dimensional electron distributions measured in (a) the magnetosphere, (b) the inner LLBL, (c) the outer LLBL/MP, and (d) the magnetosheath proper. The black, green, and blue curves denote the distributions parallel, perpendicular, and antiparallel to the magnetic field, respectively. The distributions in the LLBL/MP represent opposite streamings of hot magnetospheric electrons (antiparallel to **B**) and slightly heated magnetosheath electrons (along **B**).

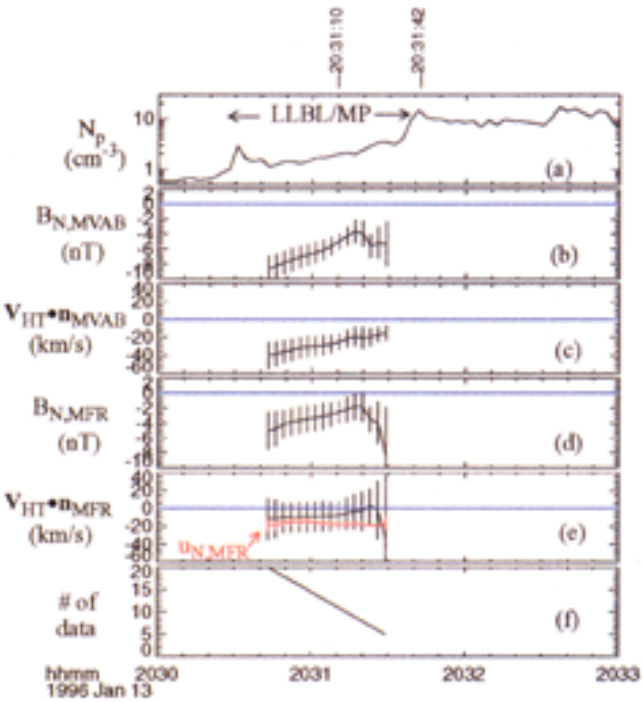

Plate 8. (a-f) Results of the variance analyses as a function of the "location" of the inner edge of the data interval. The outer edge is fixed at 2031:42 UT. When the inner edge of the interval is between 2030:42 and 2031:30 UT, both minimum variance of **B** (MVAB) and minimization of Faraday residue (MFR) methods (Plates 8b and 8d) produce a negative B_N. The minimum error in B_N occurs at 2031:10 UT for both methods. Both methods give the correct (negative) sign for the magnetopause boundary normal velocity (Plates 8c and 8e). In Plate 8e, the boundary velocity deduced directly from the MFR method [*Khrabrov and Sonnerup*, 1998b], $u_{N,MFR}$, is also plotted for comparison with $\mathbf{V}_{HT}\cdot\mathbf{n}_{MFR}$.

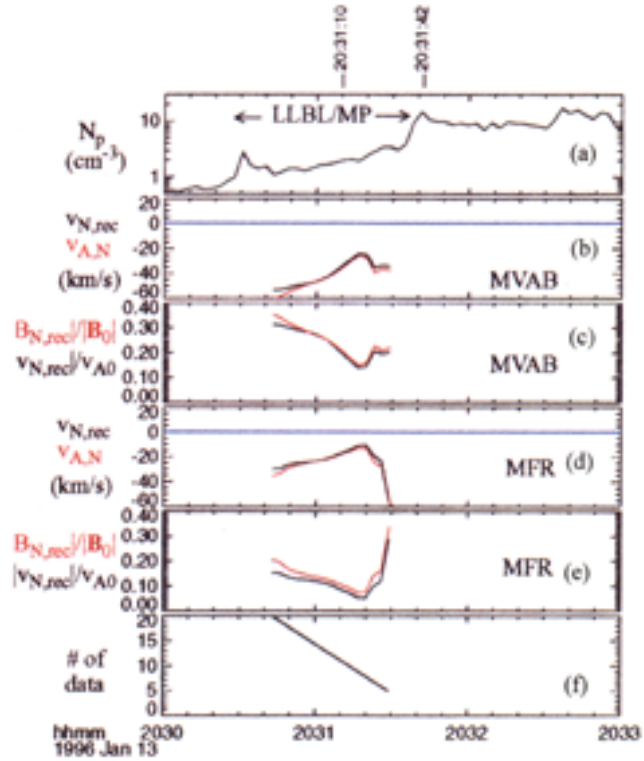

Plate 9. Results of the variance analyses as a function of the "location" of the inner edge of the data interval. The outer edge is fixed at 2031:42 UT. The agreement between the normal component of the flow velocity across the magnetopause and the normal Alfvén velocity is better than 80% for both MVAB and MFR methods.

4.6. Thicknesses of MP and LLBL

Here we deduce the MP and the combined LLBL/MP widths from the normal boundary speed ($\mathbf{V}_{HT}$•$\mathbf{n}$) and the durations of crossing of these regions. The MP is defined as the layer across which the complete field rotation (from magnetosheath to magnetospheric orientations) occurs. In this case the MP crossing lasted 20 s (2031:20-2031:40 UT). The combined LLBL/MP duration is ~ 60 s (2030:42-2030:40 UT), where we have excluded the period of boundary motion reversal before 2030:42 UT. Using the boundary speeds based on the analysis of the 2031:10-2031:42 UT interval, one obtains a MP thickness of 510 km based on MVAB and 160 km based on MFR. The combined LLBL/MP thickness is 1520 km based on MVAB and 470 km based on MFR. These thicknesses can also be expressed in terms of the gyroradius, $r_{i,\text{sheath}}$= 70 km, of the thermal magnetosheath ions (T_p= 300 eV), in the magnetospheric field (|**B**|= 25 nT). The MP thickness translates to $7r_{i,\text{sheath}}$ and $2r_{i,\text{sheath}}$, respectively, for MVAB and MFR. The corresponding combined LLBL/MP thickness is $22r_{i,\text{sheath}}$ and $7r_{i,\text{sheath}}$, respectively.

4.7. Distance to the Reconnection Site

Once B_N is known, the distance ΔL from the observation point to a stationary reconnection site can be crudely estimated [*Sonnerup et al.*, 1981] as ΔL= (|**B**|/B_N)Δs, where Δs is the distance between the MP and the inner separatrix, for which distance we use the combined LLBL/MP thickness. If the 2031:10-2031:42 UT interval is considered, the estimated reconnection site is located 1.2 R_E from the observation point based on MVAB and 0.7 R_E based on MFR. The close proximity of the X-line to the observation point is consistent with the absence of an electron edge, separated from the ion edge, discussed earlier (section 4.3). Furthermore, since the observation point was located in the Southern Hemisphere, at z_{GSM}= -6.6 R_E, and the accelerated flow is directed northward, our analysis indicates that the reconnection line at the tail flank magnetopause (x_{GSE}= -10 R_E) must have been ~ 7 R_E below the magnetic equator.

5. Discussion

5.1. Possible reasons for previously reported sub-Alfvénic flows in the MP

Although reconnection events exist in which key fluid and kinetic signatures are present and are in quantitative agreement with prediction, such events are rather rare. *Bauer et al.* [1998] found that more often than not, fluid signatures (Alfvénic flows) are observed without particle signatures (such as "D-shaped" ion distributions), and vice versa. While the present analysis does not provide an explanation for the absence of D-shaped distributions in previous accelerated flow events, it may shed light on the possible causes for the often reported sub-Alfvénic flows [e.g., *Paschmann et al.*, 1986; *Gosling et al.*, 1990a; *Phan et al.*, 1996].

We now investigate whether inadequate measurements or analysis methods could result in sub-Alfvénic flows. Previously, the flow deficiency has been attributed to a number of factors including (1) instrumental effects associated with the presence of heavy ions not resolved by the plasma instruments resulting in underestimations of the flow velocity [e.g., *Paschmann et al.*, 1986; *Gosling et al.*, 1990c; *Puhl-Quinn and Scudder,* 2000], (2) the fact that the Walén relation is derived from idealized 1-D system whereas, in reality, the system could be 2-D or 3-D [*Sonnerup et al.*, 1995]. In the event presented here the agreement between ion observations and predictions is excellent even without ion composition measurements and without taking into account additional dimensions, although such effects may be important in other events.

The present analysis suggests a possible explanation in terms of measurement resolution and analysis methods. While open field signatures (based on electron information), "D-shaped" ion distributions, and accelerated flows are detected across nearly the entire magnetopause/LLBL, the shear stress balance test of a rotational discontinuity (the Walén relation) only works for samples in the magnetopause and outer LLBL. This finding may not be surprising, since according to MHD models of dayside reconnection [e.g., *Levy et al.*, 1964], the reconnection layer consists of an outer rotational discontinuity (RD) followed by a region of uniform flow and field and then an inner slow-mode expansion fan. Thus it should be expected that while the entire reconnection layer is on open field lines, the Walén relation only applies to the magnetopause and outer LLBL regions where the rotational discontinuity controls the flow. Samples in the slow expansion fan (i.e., the inner LLBL) are not appropriate for the Walén test. Thus a fair comparison with theory is only possible if the magnetopause is well resolved by the measurements such that the RD can be identified. A previous finding that the Walén relation is better satisfied for cases with a large number of measurements within the MP/LLBL [*Phan et al.*, 1996] is consistent with this idea.

We have so far attributed flow deficits to an improper choice of data interval or too slow sampling rate. There may, however, be true physical situations where such flow deficit is expected. For example, in situations where the field lines threading the magnetopause are locally open due to prior reconnection but the reconnection process is no longer active [*Hau and Sonnerup*, 1999], open field and finite B_N signatures would be detected while the Walén test would fail. In this situation the reconnecting magnetopause is not one-dimensional but contains multiple magnetic islands and X-lines [e.g., *Shi et al.*, 1988; *Hau and Sonnerup*, 1999]. In such small-scale 2-D (or 3-D) reconnection geometries the tangential stress balance, which in 1-D geometry requires Alfvénic flows in the HT frame, can be fulfilled by variations of the total transverse pressure along the magnetopause, so that accelerated flows originated from the X-lines could be sub-Alfvénic [*Hu and Sonnerup*, 2000]. These real physical effects need to be distinguished from experimental ones in future reconnection investigations.

5.2. Occurrence of Reconnection at the Dawn Flank MP

The event presented here occurred on the dawn tail flank magnetopause. In a flank magnetopause survey by *Gosling et al.* [1986] it was found that most of the reconnection cases were detected on the duskside with few clear cases detected on the dawnside. The authors suggested that this dawn-dusk asymmetry could be due to orbital biases in the ISEE 2 data set, but it could also be a real effect caused by the way the IMF is draped around the dusk magnetosphere. However, in light of this event and a large number of cases detected by Equator-S and Geotail on the dawnside [*Phan et al.*, 2000], reconnection at the dawn tail magnetopause does not seem to be rare. Orbital biases in the ISEE 2 data set are the more likely explanation for the previously found dawn-dusk asymmetry.

The present event, as well as those reported by *Gosling et al.* [1986, 1991, 1996] and by *Phan et al.* [2000], indicates that reconnection remains active at the tail flank and high-latitude magnetopause and that its signatures are nearly identical to those observed in the subsolar region, despite the presence of high-speed shear flow in the magnetosheath. Theoretically, it has been proposed that

reconnection can occur only if the magnetosheath flow speed in the frame of the X-line is below the magnetosheath Alfvén speed [*La Belle-Hamer et al.*, 1995]. For the present event the magnetosheath flow speed (~230 km s^{-1}) in the spacecraft frame is twice the magnetosheath Alfvén speed (~120 km s^{-1}). The occurrence of reconnection in this case would not violate the theoretical prediction of *La Belle-Hamer et al.* [1995] as long as the X-line, which is estimated to be tilted ~60° relative to the equator, slides tailward along the magnetopause at a high speed (> 95 km s^{-1}). However, it is noted that at 95 km s^{-1}, our estimated distance to the X-line (0.7-1.2 R_E) would be traversed in 47-80 s. Since the v_M and v_L enhancements remain positive for more than 10 min (Plates 2d and 2e), indicating that the spacecraft stays on the same side of the X-line throughout these times, it is unlikely that such rapid motion of the X line was taking place.

6. Summary and Conclusion

We have reported a dawn tail magnetopause crossing in which key fluid and particle predictions of reconnection are verified. The measured flow acceleration, ion "D-shaped" distribution, the electron heat flux, and the presence of a finite and negative B_N all agree with predictions and are consistent with the spacecraft crossing the magnetopause in the Southern Hemisphere and tailward of the reconnection site. The combined particle and fluid signatures and their mutual consistencies provide a comprehensive set of evidence for reconnection. The quantitative agreement is remarkable, considering that the predictions (the Walén relation and the D-shaped ion distributions) are based on idealized 1-D models. On the other hand, some predicted kinetic signatures, namely reflected ions and separate ion and electron edges at the inner LLBL, were not observed in this event. The absence of the latter is consistent with our finding of close proximity (0.7-1.2 R_E) of the X-line to the observation point. The apparent absence of reflected ions implies that the percentage of these ions, which cannot be uniquely predicted theoretically, is low in some reconnection events. Despite the availability of high-resolution data and the abundant evidence for reconnection, the reconnection rate remains a difficult parameter to determine accurately: Our best estimates have an associated uncertainty of at least a factor of 2, depending on which method one employs and which data interval one picks.

The analysis of this event also reveals that while high-speed plasma jets and open field signatures are detected throughout the magnetopause and the LLBL, the rotational discontinuity condition is only satisfied in the MP and the outer part of the LLBL. This finding has implications for the analysis of reconnection events and emphasizes the need for high time sampling of the reconnection layer for accurate comparisons with theory.

Acknowledgments. We thank Ron Lepping for making his Wind and IMP 8 magnetic field data and calibration available. We also thank Karolen Paularena for providing IMP-8 magnetosheath plasma data. We thank Marit Øieroset for her comments on the manuscript. We also thank both referees for their constructive comments. This research was funded by NASA grant NAG5-6928 at U. C. Berkeley and NASA grant NAG5-7185 at Dartmouth College.

Hiroshi Matsumoto thanks J. Gosling and another referee for their assistance in evaluating this paper.

References

Bauer, T. M., G. Paschmann, N. Sckopke, W. Baumjohann, R. A. Treumann, and T. D. Phan, AMPTE-IRM observations of particle and fields at the dayside low-latitude magnetopause, in *Geospace Mass and Energy Flow: Results From the International Solar-Terrestrial Physics Program, Geophys. Monog. Ser.*, vol. 104, edited by J. L. Horwitz, D. L. Gallagher, and W. K. Peterson, pp.51-72, AGU, Washington, D.C., 1998.

Cowley, S. W. H., The causes of convection in the Earth's magnetosphere: A review of developments during the IMS, *Rev. Geophys.*, *20*, 531, 1982.

Cowley, S. W. H., Evidence for the occurrence and importance of reconnection between the Earth's magnetic field and the interplanetary magnetic field, in *Magnetic Reconnection in Space and Laboratory Plasmas, Geophys. Monog. Ser.*, vol. 30, edited by E. W. Hones, pp. 375-378, AGU, Washington, D.C., 1984.

Dungey, J. W., Interplanetary magnetic field and the auroral zones, *Phys. Rev. Lett.*, *6*, 47, 1961.

Fairfield, D. H., Average and unusual locations of the Earth's magnetopause and bow shock, *J. Geophys. Res.*, *76*, 6700, 1971.

Fujimoto, M., A. Nishida, T. Mukai, Y. Saito, T. Yamamoto, and S. Kokubun, Plasma sheet entry from the flanks of the near-Earth magnetotail: Geotail observations in the dawnside LLBL and the plasma sheet, *J. Geomagn. Geoelectr.*, *48*, 711, 1996.

Fuselier, S. A., D. M. Klumpar, and E. G. Shelly, Ion reflection and transmission during reconnection at the Earth's subsolar magnetopause, *Geophys. Res. Lett.*, *18*, 139, 1991.

Gosling, J. T., J. R. Asbridge, S. J. Bame, W. C. Feldman, G. Paschmann, N. Sckopke, and C. T. Russell, Evidence for quasi-stationary reconnection at the dayside magnetopause, *J. Geophys. Res.*, *87*, 2147, 1982.

Gosling, J. T., M. F. Thomsen, S. J. Bame, and C. T. Russell, Accelerated plasma flows at the near-tail magnetopause, *J. Geophys. Res.*, *91*, 3029, 1986.

Gosling, J. T., M. F. Thomsen, S. J. Bame, R. C. Elphic, and C. T. Russell, Plasma flow reversals at the dayside magnetopause and the origin of asymmetric polar cap convection, *J. Geophys. Res.*, *95*, 8073, 1990a.

Gosling, J. T., M. F. Thomsen, S. J. Bame, T. G. Onsager, and C. T. Russell, The electron edge of the low-latitude boundary layer during accelerated flow events, *Geophys. Res. Lett.*, *17*, 1833, 1990b.

Gosling, J. T., M. F. Thomsen, S. J. Bame, R. C. Elphic, and C. T. Russell, Cold ion beams in the low-latitude boundary layer during accelerated flow events, *Geophys. Res. Lett.*, *17*, 2245, 1990c.

Gosling, J. T., M. F. Thomsen, S. J. Bame, R. C. Elphic, and C. T. Russell, Observations of reconnection of interplanetary and lobe magnetic field lines at the high-latitude magnetopause, *J. Geophys. Res.*, *96*, 14,097, 1991.

Gosling, J. T., M. F. Thomsen, G. Le, and C. T. Russell, Observations of reconnection at the lobe magnetopause, *J. Geophys. Res.*, *101*, 24,765, 1996.

Hau, L.-N., and B. U. Ö. Sonnerup, Two-dimensional coherent structures in the magnetopause: Recovery of static equilibria from single-spacecraft data, *J. Geophys. Res.*, *104*, 6899, 1999.

Hu, Q., and B. U. Ö. Sonnerup, Magnetopause transects from two spacecraft: A comparison, *Geophys. Res. Lett.*, *27*, 1443, 2000.

Khrabrov, A. V., and B. U. Ö. Sonnerup, Error estimates for minimum variance analysis, *J. Geophys. Res.*, *103*, 6641, 1998a.

Khrabrov, A. V., and B. U. Ö. Sonnerup, Orientation and motion of current layers: Minimization of the Faraday residue, *Geophys. Res. Lett.*, *25*, 2373, 1998b.

Khrabrov, A. V., and B. U. Ö. Sonnerup, DeHoffmann-Teller analysis, in *Analysis Methods for Multi-spacecraft Data*, edited by G. Paschmann and P. W. Daly, *ISSI Sci. Rep., SR-001*, p. 221-248, ESA Publications Division, Noordwijk, The Netherlands, 1998c.

La Belle-Hamer, A. L., A. Otto, and L. C. Lee, Magnetic reconnection in the presence of sheared flow and density asymmetry: Applications to the Earth's magnetopause, *J. Geophys. Res.*, *100*, 11,875, 1995.

Lepping, R. P., et al., The Wind magnetic field investigation, *Space Sci. Rev.*, *71*, 207, 1995.

Levy, R. H., H. E. Petschek, and G. L. Siscoe, Aerodynamic aspects of the magnetospheric flow, *AIAA J.*, *2*, 2065, 1964.

Lin, R. P., et al., A three-dimensional plasma and energetic particle investigation for the Wind spacecraft, *Space Sci. Rev.*, *71*, 125, 1995.

Lindqvist, P. -A., and F. S. Mozer, The average tangential electric field at the noon magnetopause, *J. Geophys. Res.*, *95*, 17,137, 1990.

Mitchell, D. G., F. Kutchko, D. J. Williams, T. E. Eastman, L. A. Frank, and C. T. Russell, An extended study of the low-latitude boundary layer on the dawn and dusk flanks of the magnetosphere, *J. Geophys. Res.*, *92*, 7394, 1987.

Ogilvie, K. W., R. J. Fitzenreiter, and J. D. Scudder, Observations of electron beams in the low-latitude boundary layer, *J. Geophys. Res.*, *89*, 10,723, 1984.

Papamastorakis, I., et al., The magnetopause as a tangential discontinuity, *J. Geophys. Res., 89*, 127, 1984.

Paschmann, G., B. U. Ö. Sonnerup, I. Papamastorakis, N. Sckopke, G. Haerendel, S. J. Bame, J. R. Asbridge, J. T. Gosling, C. T. Russell, and R. C. Elphic, Plasma acceleration at the Earth's magnetopause: Evidence for magnetic reconnection, *Nature, 282*, 243, 1979.

Paschmann, G., I. Papamastorakis, W. Baumjohann, N. Sckopke, C. W. Carlson, B. U. Ö Sonnerup, and H. Lühr, The magnetopause for large magnetic shear: AMPTE/IRM observations, *J. Geophys. Res., 91*, 11,099, 1986.

Phan, T. D., G. Paschmann, and B. U. Ö. Sonnerup, Low-latitude magnetopause and boundary layer for high magnetic shear, 2, Occurrence of magnetic reconnection, *J. Geophys. Res., 101*, 7817, 1996.

Phan, T.-D., et al., Low-latitude dusk flank magnetosheath, magnetopause, and boundary layer for low magnetic shear: Wind observations, *J. Geophys. Res., 102*, 19,883, 1997.

Phan, T. D., et al., Extended magnetic reconnection at the Earth's magnetopause from detection of bi-directional jets, *Nature, 404*, 848, 2000.

Puhl-Quinn, P., and J. D. Scudder, Effects of composition on Walén tests using E/Z spectrometer data, *J. Geophys. Res., 105*, 7617, 2000.

Scholer, M., and F. M. Ipavich, Interaction of ring-curent ions with the magnetopause, *J. Geophys. Res., 88*, 6937, 1983.

Shi, Y., C. C. Wu, and L. C. Lee, A study of multiple X line reconnection at the dayside magnetopause, *Geophys. Res. Lett., 15*, 295, 1988.

Smith, M. F., and D. J. Rodgers, Ion distributions at the dayside magnetopause, *J. Geophys. Res., 96*, 11,617, 1991.

Sonnerup, B. U. Ö., and L. J. Cahill Jr., Magnetopause structure and attitude from Explorer 12 observations, *J. Geophys. Res., 72*, 171, 1967.

Sonnerup, B. U. Ö., and B. G. Ledley, Electromagnetic structure of the magnetopause and boundary layer, in *Magnetospheric Boundary Layers, Eur. Space Agency Spec. Publ., ESA SP-148*, 401-420, 1979.

Sonnerup, B. U. Ö., and M. Scheible, Minimum and maximum variance analysis, in *Analysis Methods for Multi-spacecraft Data*, edited by G. Paschmann and P. W. Daly, *ISSI Sci. Rep., SR-001*, p. 185-220, ESA Publications Division, Noordwijk, The Netherlands, 1998.

Sonnerup, B. U. Ö., G. Paschmann, I. Papamastorakis, N. Sckopke, G. Haerendel, S. J. Bame, J. R. Asbridge, J. T. Gosling, and C. T. Russell, Evidence for magnetic reconnection at the Earth's magnetopause, *J. Geophys. Res., 86*, 10,049, 1981.

Sonnerup, B. U. Ö., I. Papamastorakis, G. Paschmann, and H. Luehr, Magnetopause properties from AMPTE/IRM observations of the convective electric field: Method development, *J. Geophys. Res., 92*, 12,137, 1987.

Sonnerup, B. U. Ö., G. Paschmann, and T. D. Phan, Fluid aspects of reconnection at the magnetopause: In situ observations, in *Physics of the Magnetopause, Geophys. Monog. Ser.*, vol. 90, edited by P. Song, B. U. Ö. Sonnerup, M. F. Thomsen, p. 167-180, AGU, Washington, D.C., 1995.

Terasawa, T., et al., On the determination of a moving MHD structure: Minimization of the residue of integrated Faraday's equation, *J. Geomagn. Geoelectr., 48*, 603, 1996.

Traver, D. P., D. G. Mitchell, D. J. Williams, and L. A. Frank, Two encounters with the flank low-latitude boundary layer: Further evidence for closed-field topology and investigation of the internal structure, *J. Geophys. Res., 96*, 21,025, 1991.

R. P. Lin and T. D. Phan, Space Sciences Laboratory, University of California, Berkeley, Centennial Dr. at Grizzly Peak Blvd., Berkeley, CA 94720-7450, USA (phan@ssl.berkeley.edu)

B. U. Ö Sonnerup, Thayer School of Engineering, Dartmouth College, Hanover, NH 03755-8000, USA.

(Received December 7, 2000; revised April 10, 2001;
accepted April 10, 2001.)